Published in final edited form as:
J Control Release. 2014 January 10; 173: 148–157. doi:10.1016/j.jconrel.2013.10.032.

Aluminum hydroxide nanoparticles show a stronger vaccine adjuvant activity than traditional aluminum hydroxide microparticles

Xinran Li, **Abdulaziz M. Aldayel**, and **Zhengrong Cui***
The University of Texas at Austin, College of Pharmacy, Pharmaceutics Division, Austin, TX 78712

Abstract

Aluminum hydroxide is used as a vaccine adjuvant in various human vaccines. Unfortunately, despite its favorable safety profile, aluminum hydroxide can only weakly or moderately potentiate antigen-specific antibody responses. When dispersed in an aqueous solution, aluminum hydroxide forms particulates of 1–20 μm. There is increasing evidence that nanoparticles around or less than 200 nm as vaccine or antigen carriers have a more potent adjuvant activity than large microparticles. In the present study, we synthesized aluminum hydroxide nanoparticles of 112 nm. Using ovalbumin and *Bacillus anthracis* protective antigen protein as model antigens, we showed that protein antigens adsorbed on the aluminum hydroxide nanoparticles induced a stronger antigen-specific antibody response than the same protein antigens adsorbed on the traditional aluminum hydroxide microparticles of around 9.3 μm. The potent adjuvant activity of the aluminum hydroxide nanoparticles was likely related to their ability to more effectively facilitate the uptake of the antigens adsorbed on them by antigen-presenting cells. Finally, the local inflammation induced by aluminum hydroxide nanoparticles in the injection sites was milder than that induced by microparticles. Simply reducing the particle size of the traditional aluminum hydroxide adjuvant into nanometers represents a novel and effective approach to improve its adjuvanticity.

Keywords

Vaccine; nanoparticles; microparticles; antibody responses; local inflammation

1. Introduction

Many vaccines and antigens require an adjuvant to induce a strong immune response [1]. Aluminum–containing adjuvants are approved by the United States Food and Drug Administration for human use. There are two main aluminum-containing adjuvants, aluminum hydroxide and aluminum phosphate. Aluminum hydroxide adjuvant is composed of small primary fibers with an average calculated dimension of 4.5 × 2.2 × 10 nm, whereas the primary particles of aluminum phosphate adjuvant are around 50 nm [2]. In an aqueous solution, however, the size of the primary particles of both aluminum hydroxide and

***Correspondence to:** Zhengrong Cui, Ph.D., Tel: (512) 495-4758, Fax: (512) 471-7474, zhengrong.cui@austin.utexas.edu.

aluminum phosphate becomes 1– 20 μm as a result of aggregation [3]. The mechanisms of immunopotentiation by aluminum-containing adjuvants have yet been fully elucidated. Originally, it was proposed that aluminum-containing adjuvants could form an antigen depot in the injection site, from where the antigens are slowly released, and thereby the adsorption efficiency of antigens on aluminum-containing adjuvants is thought to be critical [1]. However, data from Hansen *et al*. (2007) showed that the tight binding of antigens onto aluminum-containing adjuvants may significantly reduce the amount of antigens that can elute from the aluminum salts, resulting in a weak antibody response [4]. Berthold *et al*. (2005) examined whether the full adsorption of antigens onto adjuvants is necessary by comparing the immune responses induced by two vaccine formulations: *B. anthracis* recombinant protective antigen (PA) protein adsorbed onto aluminum hydroxide with a high binding efficiency, and PA admixed with aluminum phosphate with a negligible binding [5]. It was found that both formulations induced comparable anti-PA antibody responses, suggesting that the adjuvant activity of aluminum salts may not be entirely depended on the adsorption of the antigens onto the adjuvants [5]. Other mechanisms of immunopotentiation by aluminum-containing adjuvants have been proposed as well [2, 6, 7]. HogenEsch (2002) summarized that aluminum-containing adjuvants may enhance immune responses by (i) direct or indirect stimulation of dendritic cells (DCs) [8]; (ii) activation of complements [9]; and (iii) induction of the release of chemokines [6, 9]. More recently, aluminum-containing adjuvants have been shown to promote caspase-1 activation and IL-1β secretion through the NALP3 inflammasomes [10].

Due to their favorable safety profile, aluminum-containing adjuvants have been widely used in human vaccines for decades. Unfortunately, aluminum-containing adjuvants can only weakly or moderately potentiate antigen-specific antibody responses and are generally considered incapable of helping antigens to induce cellular immune responses [11]. As aforementioned, when dispersed in an aqueous solution, both aluminum hydroxide and aluminum phosphate form 1–20 μm particulates [3]. Recently, there had been extensive efforts in identifying the relationship between the size of particulate vaccine carriers and their adjuvant activities [12–14]. Although it remains controversial as to what particle size is associated with the most potent adjuvant activity, it is clear that the size of particulate vaccine carriers significantly affects their adjuvant activities, and there are data showing that particulate vaccine carriers of around 200 nm (or less) may be optimal. For examples, Fifis *et al*. (2004) reported that ovalbumin (OVA)-conjugated polystyrene particles of 230 nm induced stronger OVA-specific antibody and cellular immune responses than other larger OVA-conjugated polystyrene particles after intradermally injected into mice [13, 15]. In a previous study, we also showed that small solid lipid nanoparticles of 200 nm have a more potent adjuvant activity than larger solid lipid nanoparticles of 700 nm, when OVA as an antigen is surface-conjugated on them [16]. The ability of the smaller nanoparticles to more effectively facilitate the uptake of antigens carried by them by antigen-presenting cells (APCs) and to up-regulate the expression of major histocompatibility complex and co-stimulatory molecules is likely related to their potent adjuvant activity [16]. Based on these findings, we proposed to improve the adjuvant activity of the traditional aluminum-containing adjuvants by reducing their particle size. We hypothesized that small aluminum hydroxide nanoparticles of ≤ 200 nm have a more potent vaccine adjuvant activity than the traditional aluminum hydroxide adjuvant with a particle size of 1–20 μm. To test this hypothesis, we synthesized aluminum hydroxide nanoparticles with a mean diameter of 112 nm and compared their adjuvant activity with that of the traditional aluminum hydroxide suspension with a mean diameter of 9.3 μm. OVA and *B. anthracis* PA protein were used as model antigens.

2. Materials and Methods

2.1. Materials

Dried aluminum hydroxide gel was from Spectrum (Gardena, CA). Aluminum chloride hexahydrate, sodium hydroxide, OVA, horse serum, Laemmli sample buffer, fluorescein-5(6)-isothiocyanate (FITC), sodium bicarbonate, sodium carbonate, phosphate-buffered saline (PBS), and incomplete Freund's adjuvant (IFA) were from Sigma-Aldrich (St. Louis, MO). Goat anti-mouse immunoglobulins (IgG) were from Southern Biotechnology Associates, Inc. (Birmingham, AL). Carbon-coated 400-mesh grids were from Electron Microscopy Sciences (Hatfield, PA). Vectashield mounting medium with 4', 6-diamidino-2-phenylindole (DAPI) was from Vector Laboratories, Inc. (Burlingame, CA). *B. anthracis* PA protein was from List Biological Laboratories, Inc. (Campbell, CA). Bio-safe™ Coomassie blue staining solution and Bio-Rad DC™ protein assay reagents were from Bio-Rad Laboratories (Hercules, CA). GM-CSF was from R&D Systems, Inc. (Minneapolis, MN). Tissue-Tek® O.C.T. compound medium was from Sakura Finetek USA, Inc. (Torrance, CA). Cell culture medium and fetal bovine serum (FBS) were from Invitrogen (Carlsbad, CA).

2.2. Mice and cell lines

Female BALB/c and C57BL/6 mice, 6–8 weeks of age, were from Charles River Laboratories, Inc. (Wilmington, MA). The OVA-expressing B16-OVA cell line was generously provided by Dr. Edith M. Lord and Dr. John Frelinger (University of Rochester Medical Center, Rochester, NY) [17] and cultured in RPMI1640 medium supplemented with 5% FBS and 400 μg/ml of geneticin (Sigma). Mouse J774A.1 macrophage cells (# TIB-67™) were from the American Type and Culture Collection (Manassas, VA) and grown in DMEM supplemented with 10% FBS, 100 U/ml of penicillin and 100 μg/ml of streptomycin, all from Invitrogen. DC2.4 cells (a mouse dendritic cell line) were originally created by Dr. Kenneth Rock (University of Massachusetts Medical School, Worcester, MA) [18] and grown in RPMI1640 medium supplemented with 10% FBS, 100 U/ml of penicillin and 100 μg/ml of streptomycin.

2.3. Preparation of aluminum hydroxide nanoparticles and microparticles

Aluminum hydroxide nanoparticles of less than 200 nm were synthesized by reacting aluminum chloride with sodium hydroxide in a solution. An equal volume of a 3.6 mg/ml $AlCl_3 \cdot 6H_2O$ solution and a 0.04 M NaOH solution were added into a glass vial, and a small volume of 0.01 M NaOH was added to adjust the pH to 7.0. After 20 min of stirring at room temperature, the particle suspension was sonicated for 15 min to break down the particle size. A PD10 desalting column (Amersham Biosciences, Piscataway, NJ) was then used to remove the sodium chloride in the suspension, and the eluted fractions were analyzed for nanoparticles by measuring the particle size using a Malvern Zetasizer Nano ZS (Westborough, MA), and for aluminum content using a Varian 710-ES Inductively Coupled Plasma Optical Emission Spectrometer in the Civil Architectural and Environmental Engineering Department at the University of Texas at Austin. The fourth fraction with the highest concentration of aluminum was used for further studies. Endotoxin was not detectable in the nanoparticle preparation with a ToxinSensor™ chromogenic limulus amebocyte lysate endotoxin assay kit from GenScript (Piscataway, NJ) [16]. Aluminum hydroxide microparticles were prepared by dispersing dried aluminum hydroxide gel into sterile water, followed by vigorous vortexing and 5 min of water-bath sonication, if needed. The size of the microparticles was determined using a Sympatec Helos laser diffraction instrument (Sympatec GmbH, Germany) equipped with a R3 lens.

2.4. Stability of aluminum hydroxide particles

The stability of aluminum hydroxide particles in suspension at 4°C or room temperature was initially examined before adsorption with proteins. The particles in suspension were kept at 4°C for 30 days, and their sizes were measured on days 0 and 30. In another study, the particles in suspension were kept at room temperature for 15 days, and their sizes were measured on days 0, 1, 7 and 15.

2.5. X-ray diffraction

The X-ray diffractograms of aluminum hydroxide particles were obtained with a Scintag X1 theta-theta powder diffractometer using Cu K-alpha radiation and a solid state Si(Li) detector in the Texas Materials Institute X-Ray Facility in the Chemical Engineering Department at the University of Texas at Austin.

2.6. Adsorption of protein antigens on aluminum hydroxide particles

The adsorption of proteins (OVA or PA) on aluminum hydroxide particles was carried out by mixing the particles in suspension with the protein in solution. Briefly, a certain volume of the protein solution was added into a tube (10 μg OVA or 4 μg PA), followed by the addition of particles in suspension at a weight ratio of 1:5 to 1:1 (OVA vs. particles) or 1:5 (PA vs. particles). After 20 min of gentle stirring, the protein-particle mixtures were stored at 4°C or freeze-dried, if needed, before further use.

The OVA-adsorbed aluminum hydroxide nanoparticles were lyophilized using a FreeZone plus 4.5 liter cascade console freeze dry system (Labconco, Kansas City, MO). A proper cryoprotectant such as trehalose (2%, w/v) was needed to successfully freeze-dry the nanoparticles (Fig. S1A). In a short-term 28-day study and when stored as a lyophilized powder at 4°C, the size of the lyophilized, OVA-adsorbed aluminum hydroxide nanoparticles did not significantly change (Fig. S1B), indicating that the antigen-adsorbed aluminum hydroxide nanoparticles may be stored long-term as a lyophilized powder.

2.7. Transmission electron microscopy (TEM)

The OVA-adsorbed aluminum hydroxide nanoparticles were examined using an FEI Tecnai Transmission Electron Microscope in the Institute for Cellular and Molecular Biology (ICMB) Microscopy and Imaging Facility at The University of Texas at Austin [19]. Carbon-coated 400-mesh grids were activated for 1–2 min. One drop of the OVA-adsorbed nanoparticle suspension was deposited on the grids and incubated for 2 min at room temperature. The grids were washed with water and dried for 1 min. Extra water was removed using filter paper. The grids were then stained with uranyl acetate for 2 min, washed with water, and allowed to dry for 15 min before observation.

2.8. Scanning electron microscope (SEM)

The OVA-adsorbed aluminum hydroxide nanoparticles and microparticles were examined using a Zeiss Supra 40 VP Scanning Electron Microscope in the ICMB Microscopy and Imaging Facility. One drop of aluminum hydroxide particle suspension was deposited on the specimen stub using a double stick carbon tape and allowed to dry overnight. The specimen stubs with samples were then placed in the sputter coater chamber and coated with a very thin film of iridium before SEM examination [20].

2.9. SDS-PAGE

SDS-PAGE assay was used to determine the extent to which the protein antigen was bound onto the aluminum hydroxide particles. Briefly, OVA (10 μg) was mixed with various amounts of aluminum hydroxide particles in suspension (0, 1, 2, 5, 10, 20, 50, and 100 μg).

The OVA-particle mixtures were then lyophilized. The resultant powders were reconstituted in de-ionized water and mixed with Laemmli sample buffer (62.5 mM Tris-HCl, pH 6.8, 25% glycerol, 2% SDS, and 0.01% Bromophenol Blue). Electrophoresis was performed with 7.5% Mini-PROTEAN® TGX™ precast polyacrylamide gels (Bio-Rad). Precision plus protein standards were run along with the samples at 130 V for 1 h. The gels were stained in a Bio-Safe Coomassie blue staining solution and scanned using a Kodak Image Station (Rochester, NY).

2.10. Preparation of bone marrow dendritic cells

Bone marrow dendritic cells (BMDCs) were generated from bone marrow precursors from C57BL/6 mice [21]. Briefly, femur bones were removed from C57BL/6 mice and purified from surrounding tissues. The bones were left in 70% ethanol for 2 min for disinfection and washed with sterile PBS. After both ends of femur bones were removed, bone marrow was flushed out with PBS using a hypodermic needle attached to a syringe. After 3 washes with PBS, all leukocytes obtained were transferred into bacteriological petri dishes and cultured with 10 ml of RPMI1640 medium supplemented with 10% FBS, 100 U/ml of penicillin, 100 μg/ml of streptomycin, 2-mercaptomethanol (50 μM) and granulocyte-macrophage-colony stimulating factor (GM-CSF) (100 ng/ml). Cells were allowed to grow at 37°C under 5% CO_2 for 3 days, and another 10 ml of culture medium was added into the original dish. On day 6, half of the supernatant was collected and centrifuged at 800 rpm for 4 min. Cell pellet was re-suspended in culture medium and added back into the original dish. Cells on days 7 or 8 were used for further studies. In order to examine the purity of BMDCs, the cells were stained with antibodies against CD11c (BD Pharmingen, San Diego, CA) [21], and analyzed using a Guava EasyCyte 8HT microcapillary flow cytometer (Millipore Corporation, Hayward, CA). A high purity of 86.5% BMDCs was obtained after 8 days in culture medium.

2.11. Uptake of the OVA-adsorbed particles by BMDCs, DC2.4 cells and J774A.1 cells in culture

In vitro uptake studies were carried out using OVA that was pre-labeled with FITC [16]. BMDCs, DC2.4 or J774A.1 cells (50,000 cells/well) were seeded into 24-well plates and allowed to grow overnight at 37°C, 5% CO_2. FITC-labeled OVA-particles were added into the cell culture and incubated at 37°C under 5% CO_2 or at 4°C. After further incubation (3 h for DC2.4 and J774A.1 cells, 6 h for BMDCs), cells were washed with PBS (10 mM, pH 7.4) three times, lyzed with Triton X-100 (0.17%, v/v) and then applied to a BioTek Synergy HT microplate reader to measure the fluorescence intensity. Endocytosis is inhibited at 4°C. Therefore, a subtraction of the fluorescence intensity of the cells incubated at 4°C from the fluorescence intensity of the cells incubated at 37°C, 5% CO_2, allowed us to estimate the amount of FITC-OVA that was internalized.

2.12. Fluorescence microscopy

DC2.4 cells (1.5×10^4) were plated on poly-D-lysine-coated glass coverslips overnight. FITC-labeled OVA-adsorbed particles were added and incubated with the cells for 30 to 60 min at 37°C, 5% CO_2. Cells were then washed with PBS, fixed in 3% paraformaldehyde for 20 min at room temperature, followed by three times of wash with PBS. Coverslips were mounted on the slides using Vectashield mounting medium with DAPI. Fluorescent images were acquired using an Olympus BX60 Biological Microscope (Center Valley, PA).

2.13. Immunization studies

All animal studies were carried out following National Institutes of Health guidelines for care and use of laboratory animals. The animal protocol was approved by the Institutional

Animal Care and Use Committee at The University of Texas at Austin. When OVA was used as the antigen, female BALB/c mice (18–20 g) were subcutaneously injected with OVA-adsorbed aluminum hydroxide particles once a week for three consecutive weeks. The dose of the OVA was 10 μg per mouse per injection; 20 (or 50) μg per mouse per injection for the particles. Sterile PBS or OVA (10 μg) dissolved in PBS was used as controls. Twenty seven days after the first dose, mice were bled for antibody assay. When PA was used as the antigen, female BALB/c mice (18–20 g) were immunized subcutaneously with PA-adsorbed aluminum hydroxide particles on days 0 and 14. As negative controls, mice were injected with sterile PBS or PA alone. The dose of PA was 4 μg per mouse per injection, and the dose of the particles was 20 μg per mouse per injection. Mice were bled one week and one month after the second immunization for antibody assay. Specific antibody levels in serum samples were determined using enzyme-linked immunosorbent assay (ELISA) as previously described [19].

2.14. Tumor prevention assays

Female C57BL/6 mice (18–20 g) were immunized with OVA-adsorbed particles, PBS, or OVA alone on days 0, 7, and 14 by subcutaneous injection. The dose of OVA was 10 μg per mouse per injection, and the particles were 20 μg. As a positive control, mice were also immunized with OVA adjuvanted with IFA (50 μl per mouse per injection). On day 21, B16-OVA cells (50,000/mouse) were subcutaneously injected in the right flank of the mice (different from the sites of immunization). Tumor growth was monitored daily. Tumor size was measured using a caliper, and the volume was calculated using the following equation [22]: tumor volume (mm^3) = 1/2 [length × $(width)^2$]

2.15. Histological examination

BALB/c mice were injected with PA adsorbed aluminum hydroxide particles on day 0 and 19. As negative controls, mice were injected with sterile PBS or PA alone. On day 40, mice were euthanized for histological examination. The hair on the injection site was initially removed using Nair® lotion (Church and Dwight Co, Princeton, NJ). The skin at the injection sites, including skin and muscle tissues, were removed and spread out on a piece of index paper. The tissue and paper together were cut into a 1 cm × 1 cm square and transferred to tissue cryomolds (25 mm × 20 mm × 5 mm, Sakura Finetek USA, Inc.). Any residual spaces in the cryomolds were filled with Tissue-Tek® O.C.T. compound medium and fixed in the vapor of liquid nitrogen for 10 min. After the O.C.T. compound medium was frozen into a solid white color, the whole cryomoles were removed and wrapped with aluminum foil. The prepared samples were stored at −80 °C for cryostat sectioning and staining with Hematoxylin and eosin (H&E, Sigma, St. Louis, MO) in the Histology and Tissue Analysis Facility in the Dell Pediatric Research Institute, University of Texas at Austin [23].

2.16. Statistics

Statistical analyses were completed using analysis of variance followed by Fisher's protected least significant difference procedure. A p-value of ≤ 0.05 (two-tail) was considered statistically significant.

3. Result and Discussion

3.1. Synthesis and characterization of aluminum hydroxide particles

In order to evaluate the effect of the size of aluminum hydroxide particles on their adjuvant activity, aluminum hydroxide nanoparticles and microparticles with mean diameters of 112 ± 6.2 nm and 9.3 ± 2.2 μm, respectively, were prepared (Fig. 1A). At neutral pH, the zeta

potentials of both particles were positive (Fig. 1A), but the zeta potential of the aluminum hydroxide microparticles was less positive than that of the aluminum hydroxide nanoparticles (Fig. 1A). The positive charge of aluminum hydroxide particles was likely due to the metallic hydroxyls on their surface, which could accept protons and show a positive zeta potential [24]. Since the reduction of particle size increases the total surface area of the particles [25], the aluminum hydroxide nanoparticles are expected to have a relatively larger surface area than the microparticles, and thus more metallic hydroxyl groups on their surface, resulting in a more positive zeta potential. The aluminum hydroxide nanoparticles were stable when stored at 4°C (or room temperature (Fig. S2)), whereas the microparticles were slightly less stable (Fig. 1B), likely because the zeta potential of the nanoparticles was > 30 mV, whereas the zeta potential of the microparticles was < 30 mV, at which the electrostatic repulsion was not strong enough to prevent aggregation [26]. The X-ray powder patterns of aluminum hydroxide particles are shown in Figures 1C–D. The nanoparticles were completely amorphous (Fig. 1C). The microparticles were mostly crystalline $Al(OH)_3$ (Fig. 1D), although the large peak in the left indicated that some amorphous AlO(OH) materials existed as well (Fig.1D).

3.2. Characterization of OVA-adsorbed aluminum hydroxide particles

Shown in Fig. 2A are the size and zeta potentials of the aluminum hydroxide nanoparticles and microparticles after the adsorption of OVA protein at a 1:2 ratio (OVA vs. particle, w/w). The mean diameters of the OVA-adsorbed nanoparticles and microparticles were 129 ± 20 nm and 9.4 ± 1.7 μm, respectively; and their zeta potentials were 16 ± 1.8 and −23 ± 1.9, respectively. The sizes of both particles increased after the adsorption of OVA. Since OVA is net negatively charged at neutral pH (isoelectric point (pI), 4.7), after the adsorption of OVA, the zeta potentials of the resultant nanoparticles became less positive, and the zeta potential of microparticles even changed from positive to negative (Fig. 2A).

Shown in Fig. 2B are the fractions of free OVA when a fixed amount of OVA was mixed with increasing amounts of the aluminum hydroxide nanoparticles or microparticles. As expected, the fraction of unbound OVA decreased when the amount of aluminum hydroxide particles added was increased. When the ratio of OVA to nanoparticles was decreased to 1:2 and 1:5, the OVA protein bands can no longer be detected on the SDS-PAGE, indicating that all the OVA proteins were bound on the particles when OVA and nanoparticles were mixed at 1:2 ratio or lower. The adsorption of the OVA to the aluminum hydroxide microparticles was not as extensive as to the nanoparticles. Only when the weight ratio of microparticles to OVA was increased to 5:1, the OVA protein bands were no longer detectable using SDS-PAGE (Fig. 2B). The mechanisms of the adsorption of OVA to aluminum hydroxide particles are likely two-fold: (1) the electrostatic interaction between OVA and aluminum hydroxide particles because they have opposite net charges at neutral pH; and (2) ligand exchange as OVA protein contains up to two phosphate groups, which could strongly bind to aluminum instead of a hydroxyl group [27]. The higher protein adsorption capacity of the aluminum hydroxide nanoparticles is consistent with the larger total surface area of the nanoparticles, which contain more binding sites for protein adsorption. The relatively smaller total surface area of the aluminum hydroxide microparticles limited the amount of proteins adsorbed on them. Besides the effect of the surface area, the zeta potential of the aluminum hydroxide particles may also have contributed to the adsorption capacity. The zeta potential of the aluminum hydroxide nanoparticles was more positive than that of the microparticles (Fig. 1A). Therefore, the aluminum hydroxide nanoparticles may have attracted more OVA proteins to their surface.

Shown in Fig. 2C is a representative SEM picture of the OVA-adsorbed aluminum hydroxide microparticles. A representative TEM picture of the OVA-adsorbed aluminum hydroxide nanoparticles is shown in Fig. 2D. A representative SEM picture of the OVA-

adsorbed aluminum hydroxide nanoparticles is also available in Fig. S3. The nanoparticles are rod-shaped with a smooth surface, whereas the microparticles have a rough surface and are in irregular shapes.

3.3. OVA-adsorbed small aluminum hydroxide nanoparticles induced a stronger OVA-specific antibody immune response than OVA-adsorbed large aluminum hydroxide microparticles

Aluminum hydroxide particles with diameters in the range of 1–20 μm have been widely used in human vaccines [11]. Previous data showed that nanoparticles with a mean diameter of around or less than 200 nm have a more potent adjuvant activity than larger particles [16, 19]. To test whether small aluminum hydroxide nanoparticles of less than 200 nm can help an antigen to induce a stronger immune response than larger aluminum hydroxide microparticles, the anti-OVA immune responses induced by OVA-adsorbed aluminum hydroxide nanoparticles and microparticles at the OVA to particles ratio of 1:2 were compared. Data in Fig. 3A showed that the anti-OVA IgG level in mice that were immunized with the OVA-adsorbed aluminum hydroxide nanoparticles was significantly higher than that in mice that were immunized with OVA-adsorbed microparticles or OVA alone (at 100-fold dilution, $p < 0.001$, OVA-NPs vs. OVA; $p = 0.018$, OVA-NPs vs. OVA-MPs; $p = 0.05$, OVA alone vs. OVA-MPs).

There were data showing that nanoparticles as a carrier may allow proteins to induce antitumor responses. For example, Falo *et al*. (1995) evaluated the ability of particulate antigens against tumor growth and found that immunization of mice with OVA-conjugated iron beads more effectively prevented the growth of tumor cells that overexpress OVA (B16-OVA) in the immunized mice, as compared to immunization with OVA alone [28]. Falo *et al*. (1995) also concluded that the antitumor immunity was essentially contributed by specific $CD8^+$ T cells [28]. Accordingly, a tumor prevention study was carried out to evaluate the ability of our OVA-adsorbed aluminum hydroxide nanoparticles in preventing tumor growth. Twenty-one days after C57BL/6 mice were immunized with OVA-adsorbed aluminum hydroxide nanoparticles or microparticles, they were challenged with the OVA-expressing B16-OVA tumor cells, and the tumor growth was monitored. As shown in Fig. 3B, 31 days after tumor cell injection, tumors were detected only in one of the 5 mice that were immunized with the OVA-adsorbed aluminum hydroxide nanoparticles. In contrast, all mice immunized with the OVA-adsorbed microparticles or with OVA alone developed tumors, indicating that the immune responses induced by OVA-adsorbed aluminum hydroxide nanoparticles can inhibit tumor growth. However, the antitumor activity was likely antibody-mediated because we were not able to consistently detect OVA-specific $CD8^+$ T cell response in the immunized mice (data not shown).

As shown in Fig. 2B, when the ratio of particles to OVA was 1:2, the OVA protein was fully adsorbed on the nanoparticles, but the adsorption of the OVA to the aluminum hydroxide microparticles was not as extensive. Only when the microparticles to OVA weight ratio reached 5:1, the OVA protein was fully adsorbed on both nanoparticles and microparticles. To make sure that the stronger immune response induced by the OVA-adsorbed aluminum hydroxide nanoparticles shown in Fig. 3A was not due to the difference in the extent to which the OVA was adsorbed on the aluminum hydroxide nanoparticles and microparticles, another mouse immunization study was carried out by immunizing mice with OVA-adsorbed aluminum hydroxide nanoparticles or microparticles at an aluminum hydroxide to OVA weight ratio 5:1. As shown in Fig. 3C, the serum anti-OVA IgG response induced by the OVA-adsorbed aluminum hydroxide nanoparticles was still stronger than that induced by the OVA-adsorbed aluminum hydroxide microparticles ($p = 0.02$ at all three dilutions,

OVA-NPs vs. OVA-MPs), demonstrating that the stronger immune response induced by the OVA-adsorbed aluminum hydroxide nanoparticles was truly due to their smaller size.

3.4. PA-adsorbed aluminum hydroxide nanoparticles induced a stronger PA-specific antibody response than PA-adsorbed aluminum hydroxide microparticles

To test whether the potent adjuvant activity of the aluminum hydroxide nanoparticles was unique to OVA as an antigen, we completed a similar immunization study with the anthrax PA protein. Anthrax is a toxin-mediated disease, and anthrax toxin is consisted of three proteins, PA, lethal factor, and edema factor [29]. PA proteins form a heptamer on the surface of cells, from which the edema factor and lethal factor enter cells [29]. Therefore, the induction of anti-PA antibody responses is critical and sufficient for a vaccine to protect against anthrax [30]. PA was absorbed on aluminum hydroxide particles at a particle to PA ratio of 5:1 (w/w). The mean diameters of the resultant PA-adsorbed aluminum hydroxide nanoparticles and microparticles were 204 ± 25 nm and 7.1 ± 3.4 μm, respectively (Fig. 4A). Mice were then immunized with the PA-adsorbed aluminum hydroxide nanoparticles or microparticles on days 0 and 14. One week after the first dose, anti-PA IgG was not detectable in any mice (data not shown). One week after the second dose, significant anti-PA IgG responses were detected in mice that were immunized with the PA-adsorbed aluminum hydroxide nanoparticles or microparticles, but the levels of the anti-PA IgG were not different (Fig. 4B). However, four weeks after the second immunization, the anti-PA IgG level in mice that were immunized with the PA-adsorbed aluminum hydroxide nanoparticles was significantly higher than that in mice that were immunized with the PA-adsorbed aluminum hydroxide microparticles (Fig. 4C). The anti-PA IgG1 levels 4 weeks after the second immunization are shown in Fig. 4D. A significantly higher level of anti-PA IgG1 was detected in mice that were immunized with PA-adsorbed aluminum hydroxide nanoparticles than in mice that were immunized with PA-adsorbed aluminum hydroxide microparticles (Fig. 4D). PA-specific IgE was not detected 4 weeks after immunization with PA-adsorbed aluminum hydroxide nanoparticles or microparticles (data not shown). The kinetics of the total serum anti-PA IgG levels within 4 weeks after the last immunization is shown in Fig. 4E. It is clear that during the 4-week period after the second immunization, the total serum anti-PA IgG level significantly increased in mice that were immunized with the PA-adsorbed aluminum hydroxide nanoparticles ($p = 0.005$, week 1 vs. week 4), but decreased in mice that were immunized with the PA-adsorbed aluminum hydroxide microparticles ($p = 0.005$, week 1 vs. week 4).

3.5. The uptake of OVA-adsorbed aluminum hydroxide particles by antigen-presenting cells in culture

One important step for an antigen to induce an immune response is its uptake by APCs. Therefore, we evaluated the extent to which DCs and macrophages, two critical APCs, can take up OVA as an antigen adsorbed on aluminum hydroxide nanoparticles or microparticles. BMDCs, DC2.4, or J774A.1 cells in culture were incubated with fluorescein-labeled OVA adsorbed on aluminum hydroxide nanoparticles or microparticles for up to 6 h, and the % of OVA internalized by the cells was determined. As shown in Fig. 5A, in all three cell lines, more OVA was internalized when adsorbed on the aluminum hydroxide nanoparticles than when adsorbed on the aluminum hydroxide microparticles. The fluorescence microscopic pictures in Fig. 5B are also supportive of the data in Fig. 5A and may explain why the aluminum hydroxide nanoparticles were more effective than the microparticles in facilitating the uptake of OVA by DC2.4 cells. Green fluorescence signal, an indication of the location of the OVA protein, was detected only inside cells that were incubated with OVA-adsorbed aluminum hydroxide nanoparticles, but not in cells that were incubated with OVA-adsorbed aluminum hydroxide microparticles (Fig. 5B). In fact, for cells that were incubated with the OVA-adsorbed aluminum hydroxide microparticles,

almost all fluorescence signals were extracellular (Fig. 5B), and it appeared that some OVA-adsorbed aluminum hydroxide microparticles were even larger than the cells (Fig. 5B), which may explain why the OVA adsorbed on the aluminum hydroxide microparticles did not enter the cells (Fig. 5A).

Previous data showed that antigens eluted from adjuvants are taken up by DCs by macropinocytosis, while those remaining adsorbed are internalized with adjuvant particles by phagocytosis [31]. Because close to 100% of the OVA was adsorbed on the aluminum hydroxide nanoparticles, it is likely that phagocytosis or endocytosis was the predominant mechanism for the internalization of the OVA that was adsorbed on the aluminum hydroxide nanoparticles. In contrast, only less than 20% OVA was adsorbed onto the microparticles (at the OVA to particle ratio of 1:2, w/w). The small percentage of OVA that was internalized by DC2.4 cells incubated with the OVA-adsorbed aluminum hydroxide microparticles was probably from the macropinocytosis of the unbound OVA and the OVA that was eluted from the microparticles. Morefield *et al*. (2005) showed that DCs are able to internalize particles with a diameter larger than that of cells [32], but we could not find any internalization of the OVA-adsorbed aluminum hydroxide microparticles using fluorescence microscopy. Previously, Kanchan and Panda (2007) also reported that nanoparticles (200–600 nm) were more efficiently taken up by macrophages in comparison to microparticles (2–8 μm) [33]. Thus, we suspect that the ability of the aluminum hydroxide nanoparticles to more effectively facilitate the uptake of the OVA adsorbed on them by APCs is related to their potent adjuvant ability (Figs. 3–4).

Finally, a comparison of the internalization of the OVA by the macrophages (J774A.1 cells) and DCs (BMDCs and DC2.4 cells) indicated that the percentage of OVA adsorbed on the aluminum hydroxide microparticles that was internalized by the macrophages was relatively higher than by the DCs (Fig. 5A). This finding is in agreement with a previous report that macrophages can effectively take up particles larger than 500 nm, whereas DCs are more effective in taking up smaller nanoparticles (< 200 nm) [34].

3.6. Aluminum hydroxide nanoparticles induced milder local inflammation reactions than aluminum hydroxide microparticles

Aluminum adjuvants have been administered safely to humans since 1932 [35]. Adverse reactions that have been reported with vaccines adjuvanted with aluminum salts are generally local reactions including subcutaneous (s.c.) nodule, granulomatous inflammation, and sterile abscesses [36]. In order to preliminarily evaluate the safety profile of our aluminum hydroxide nanoparticles, the injection sites were examined histologically. As shown in Fig. 6, microparticles and nanoparticles both induced local cutaneous inflammation in the injection sites when examined 40 days after the last injection, but the inflammation induced by the PA-adsorbed microparticles was much more severe, as indicated by the greater number of neutrophils accumulated in the injection sites and the more pronounced epidermal hyperplasia. Clearly the aluminum hydroxide nanoparticles are less proinflammatory than the microparticles.

4. Conclusions

In the present study, we synthesized aluminum hydroxide nanoparticles with a mean diameter of 112 nm and showed that the adjuvant activity of the aluminum hydroxide nanoparticles was more potent than that of the traditional aluminum hydroxide microparticles (~9 μm). The specific antibody responses induced by protein antigens adjuvanted with the aluminum hydroxide nanoparticles were stronger and more durable than that induced by the same amount of antigens adjuvanted with the traditional aluminum hydroxide microparticles. The more potent adjuvant activity of the aluminum hydroxide

nanoparticles may be partially attributed to their ability to more extensively bind to antigens and increase the uptake of the antigens adsorbed on them by APCs. Moreover, the aluminum hydroxide nanoparticles were less proinflammatory than the microparticles in the injection sites. The new aluminum hydroxide nanoparticles have the potential to be developed into a more effective and safer adjuvant to formulate new vaccines and reformulate existing vaccines.

Supplementary Material

Refer to Web version on PubMed Central for supplementary material.

Acknowledgments

This work was supported in part by the National Institutes of Health grants (AI070538, AI078304, and Al105789) to Z. Cui. A.M.A is a King Abdullah International Medical Research Center (KAIMRC) scholar and is supported by the KAIMRC scholarship program. The authors would like to thank Dr. Hugh Smyth in the College of Pharmacy at the University of Texas at Austin for kindly allowing us to use the Sympatec Helos laser diffraction instrument available in his lab.

References

1. O'Hagan DT, MacKichan ML, Singh M. Recent developments in adjuvants for vaccines against infectious diseases. Biomol. Eng. 2001; 18:69–85. [PubMed: 11566599]
2. Romero Mendez IZ, Shi Y, HogenEsch H, Hem SL. Potentiation of the immune response to non-adsorbed antigens by aluminum-containing adjuvants. Vaccine. 2007; 25:825–833. [PubMed: 17014935]
3. Hem SL, Hogenesch H. Relationship between physical and chemical properties of aluminum-containing adjuvants and immunopotentiation. Expert Rev. Vaccines. 2007; 6:685–698. [PubMed: 17931150]
4. Hansen B, Sokolovska A, HogenEsch H, Hem SL. Relationship between the strength of antigen adsorption to an aluminum-containing adjuvant and the immune response. Vaccine. 2007; 25:6618–6624. [PubMed: 17681647]
5. Berthold I, Pombo ML, Wagner L, Arciniega JL. Immunogenicity in mice of anthrax recombinant protective antigen in the presence of aluminum adjuvants. Vaccine. 2005; 23:1993–1999. [PubMed: 15734073]
6. HogenEsch H. Mechanisms of stimulation of the immune response by aluminum adjuvants. Vaccine. 2002; 20(Suppl 3):S34–S39. [PubMed: 12184362]
7. Jones LS, Peek LJ, Power J, Markham A, Yazzie B, Middaugh CR. Effects of adsorption to aluminum salt adjuvants on the structure and stability of model protein antigens. J. Biol. Chem. 2005; 280:13406–13414. [PubMed: 15684430]
8. Mannhalter JW, Neychev HO, Zlabinger GJ, Ahmad R, Eibl MM. Modulation of the human immune response by the non-toxic and non-pyrogenic adjuvant aluminium hydroxide: effect on antigen uptake and antigen presentation. Clin. Exp. Immunol. 1985; 61:143–151. [PubMed: 3876178]
9. Ulanova M, Tarkowski A, Hahn-Zoric M, Hanson LA. The Common vaccine adjuvant aluminum hydroxide up-regulates accessory properties of human monocytes via an interleukin-4-dependent mechanism. Infect. Immun. 2001; 69:1151–1159. [PubMed: 11160013]
10. Eisenbarth SC, Colegio OR, O'Connor W, Sutterwala FS, Flavell RA. Crucial role for the Nalp3 inflammasome in the immunostimulatory properties of aluminium adjuvants. Nature. 2008; 453:1122–1126. [PubMed: 18496530]
11. Gupta RK. Aluminum compounds as vaccine adjuvants. Adv. Drug Deliv. Rev. 1998; 32:155–172. [PubMed: 10837642]
12. Gutierro I, Hernandez RM, Igartua M, Gascon AR, Pedraz JL. Size dependent immune response after subcutaneous, oral and intranasal administration of BSA loaded nanospheres. Vaccine. 2002; 21:67–77. [PubMed: 12443664]

13. Kalkanidis M, Pietersz GA, Xiang SD, Mottram PL, Crimeen-Irwin B, Ardipradja K, Plebanski M. Methods for nano-particle based vaccine formulation and evaluation of their immunogenicity. Methods. 2006; 40:20–29. [PubMed: 16997710]

14. Wendorf J, Chesko J, Kazzaz J, Ugozzoli M, Vajdy M, O'Hagan D, Singh M. A comparison of anionic nanoparticles and microparticles as vaccine delivery systems. Human Vaccines. 2008; 4:44–49. [PubMed: 18438105]

15. Fifis T, Gamvrellis A, Crimeen-Irwin B, Pietersz GA, Li J, Mottram PL, McKenzie IF, Plebanski M. Size-dependent immunogenicity: therapeutic and protective properties of nano-vaccines against tumors. J. Immunol. 2004; 173:3148–3154. [PubMed: 15322175]

16. Li XR, Sloat BR, Yanasarn N, Cui ZR. Relationship between the size of nanoparticles and their adjuvant activity: Data from a study with an improved experimental design. Eur. J. Pharm. Biopharm. 2011; 78:107–116. [PubMed: 21182941]

17. Lugade AA, Moran JP, Gerber SA, Rose RC, Frelinger JG, Lord EM. Local radiation therapy of B16 melanoma tumors increases the generation of tumor antigen-specific effector cells that traffic to the tumor. J. Immunol. 2005; 174:7516–7523. [PubMed: 15944250]

18. Shen ZH, Reznikoff G, Dranoff G, Rock KL. Cloned dendritic cells can present exogenous antigens on both MHC class I and class II molecules. J. Immunol. 1997; 158:2723–2730. [PubMed: 9058806]

19. Sloat BR, Sandoval MA, Hau AM, He Y, Cui Z. Strong antibody responses induced by protein antigens conjugated onto the surface of lecithin-based nanoparticles. J. Control. Release. 2010; 141:93–100. [PubMed: 19729045]

20. Hao AY, Geng YY, Xu Q, Lu ZY, Yu L. Study of different effects on foaming process of biodegradable PLA/starch composites in supercritical/compressed carbon dioxide. J. Appl. Polym. Sci. 2008; 109:2679–2686.

21. Lutz MB, Kukutsch N, Ogilvie AL, Rossner S, Koch F, Romani N, Schuler G. An advanced culture method for generating large quantities of highly pure dendritic cells from mouse bone marrow. J. Immunol. Methods. 1999; 223:77–92. [PubMed: 10037236]

22. Tomayko MM, Reynolds CP. Determination of subcutaneous tumor size in athymic (nude) mice. Cancer Chemothe. Pharmacol. 1989; 24:148–154.

23. Lim J, Kim Y, Lee W, Kim M, Lee EJ, Kang CS, Han K. Fresh-frozen, optimal cutting temperature (OCT) compound-embedded bone marrow aspirates: a reliable resource for morphological, immunohistochemical and molecular examinations. Int. J. Lab. Hematol. 2010; 32:e34–e39. [PubMed: 19298222]

24. Stumm, W.; Sigg, L.; Sulzberger, B. Chemistry of the solid-water interface: Processes at the mineral-water and particle-water interface in natural systems. New York: Wiley; 1992.

25. Lowell, S.; Lowell, S. Characterization of porous solids and powders: Surface area, pore size, and density. Dordrecht; Boston: Kluwer Academic Publishers; 2004.

26. Bumb AR, Bernardo CAS, Dobson M, Choyke PJ, Brechbiel P, W M. Multi-modal superparamagnetic nanoprobe: Harnessing magnetic, nuclear, and optical power for diagnostic imaging applications. NSTI-Nanotech. 2010; 3

27. Iyer S, HogenEsch H, Hem SL. Effect of the degree of phosphate substitution in aluminum hydroxide adjuvant on the adsorption of phosphorylated proteins. Pharm. Dev. Technol. 2003; 8:81–86. [PubMed: 12665200]

28. Falo LD Jr, Kovacsovics-Bankowski M, Thompson K, Rock KL. Targeting antigen into the phagocytic pathway in vivo induces protective tumour immunity. Nat. Med. 1995; 1:649–653. [PubMed: 7585145]

29. Bradley KA, Mogridge J, Mourez M, Collier RJ, Young JA. Identification of the cellular receptor for anthrax toxin. Nature. 2001; 414:225–229. [PubMed: 11700562]

30. Sloat BR, Cui Z. Evaluation of the immune response induced by a nasal anthrax vaccine based on the protective antigen protein in anaesthetized and non-anaesthetized mice. J. Pharm. Pharmacol. 2006; 58:439–447. [PubMed: 16597361]

31. Davis HL, Weeratna R, Waldschmidt TJ, Tygrett L, Schorr J, Krieg AM. CpG DNA is a potent enhancer of specific immunity in mice immunized with recombinant hepatitis B surface antigen. J. Immunol. 1998; 160:870–876. [PubMed: 9551923]

32. Morefield GL, Sokolovska A, Jiang D, HogenEsch H, Robinson JP, Hem SL. Role of aluminum-containing adjuvants in antigen internalization by dendritic cells in vitro. Vaccine. 2005; 23:1588–1595. [PubMed: 15694511]

33. Kanchan V, Panda AK. Interactions of antigen-loaded polylactide particles with macrophages and their correlation with the immune response. Biomaterials. 2007; 28:5344–5357. [PubMed: 17825905]

34. Xiang SD, Scholzen A, Minigo G, David C, Apostolopoulos V, Mottram PL, Plebanski M. Pathogen recognition and development of particulate vaccines: does size matter? Methods. 2006; 40:1–9. [PubMed: 16997708]

35. Goto N, Kato H, Maeyama J, Eto K, Yoshihara S. Studies on the toxicities of aluminium hydroxide and calcium phosphate as immunological adjuvants for vaccines. Vaccine. 1993; 11:914–918. [PubMed: 8212836]

36. Goto N, Kato H, Maeyama J, Shibano M, Saito T, Yamaguchi J, Yoshihara S. Local tissue irritating effects and adjuvant activities of calcium phosphate and aluminium hydroxide with different physical properties. Vaccine. 1997; 15:1364–1371. [PubMed: 9302746]

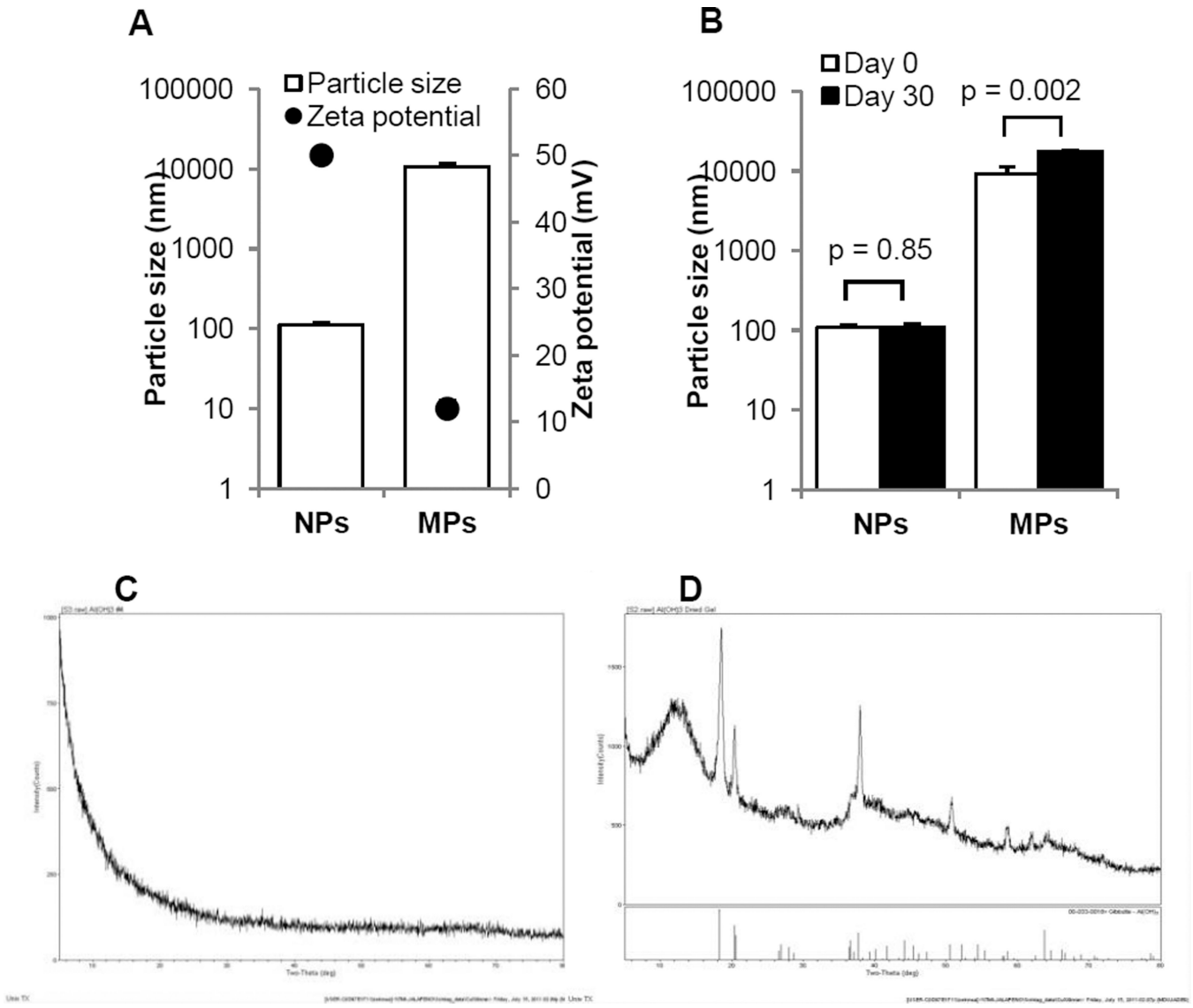

Fig. 1. Physical properties of aluminum hydroxide nanoparticles (NPs) and microparticles (MPs)

(A). Particle sizes (open bar) and zeta potentials (●).

(B). The stability of the aluminum hydroxide nanoparticles and microparticles when stored in suspension at 4°C for 30 days.

(C–D). X-ray diffractograms of aluminum hydroxide nanoparticles (C) and microparticles (D). Data shown in A and B are mean ± S.D. (n = 3).

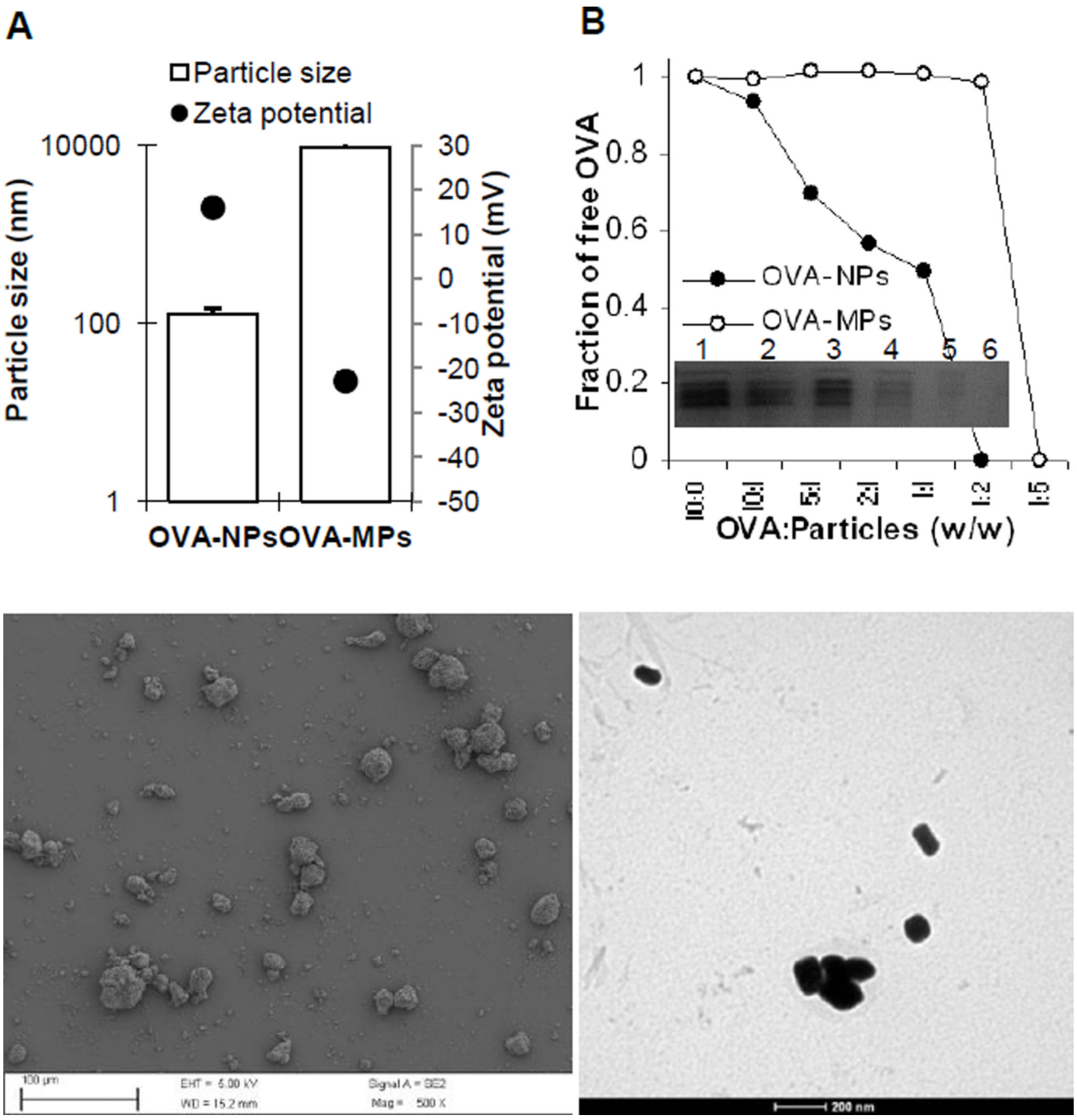

Fig. 2. Physical characterization of aluminum hydroxide nanoparticles and microparticles after adsorption of OVA

(A). Particle sizes (open bar) and zeta potentials (●) of OVA-adsorbed aluminum hydroxide nanoparticles (OVA-NPs) and OVA-adsorbed aluminum hydroxide microparticles (OVA-MPs). Data shown are mean ± S.D. (n = 3).

(B). The binding efficiency of OVA to the aluminum hydroxide nanoparticles and microparticles. Shown is the fraction of free (unbound) OVA at various OVA to particle ratios (w/w) as determined from the intensities of the protein bands on the SDS-PAGE (inset, OVA to nanoparticle ratio: lane 1, 10:0; lane 2, 10:1; lane 3, 5:1; lane 4, 2:1; lane 5, 1:1; lane 6, 1:2).

(C). A representative SEM picture of OVA-MPs.
(D). A representative TEM picture of OVA-NPs.

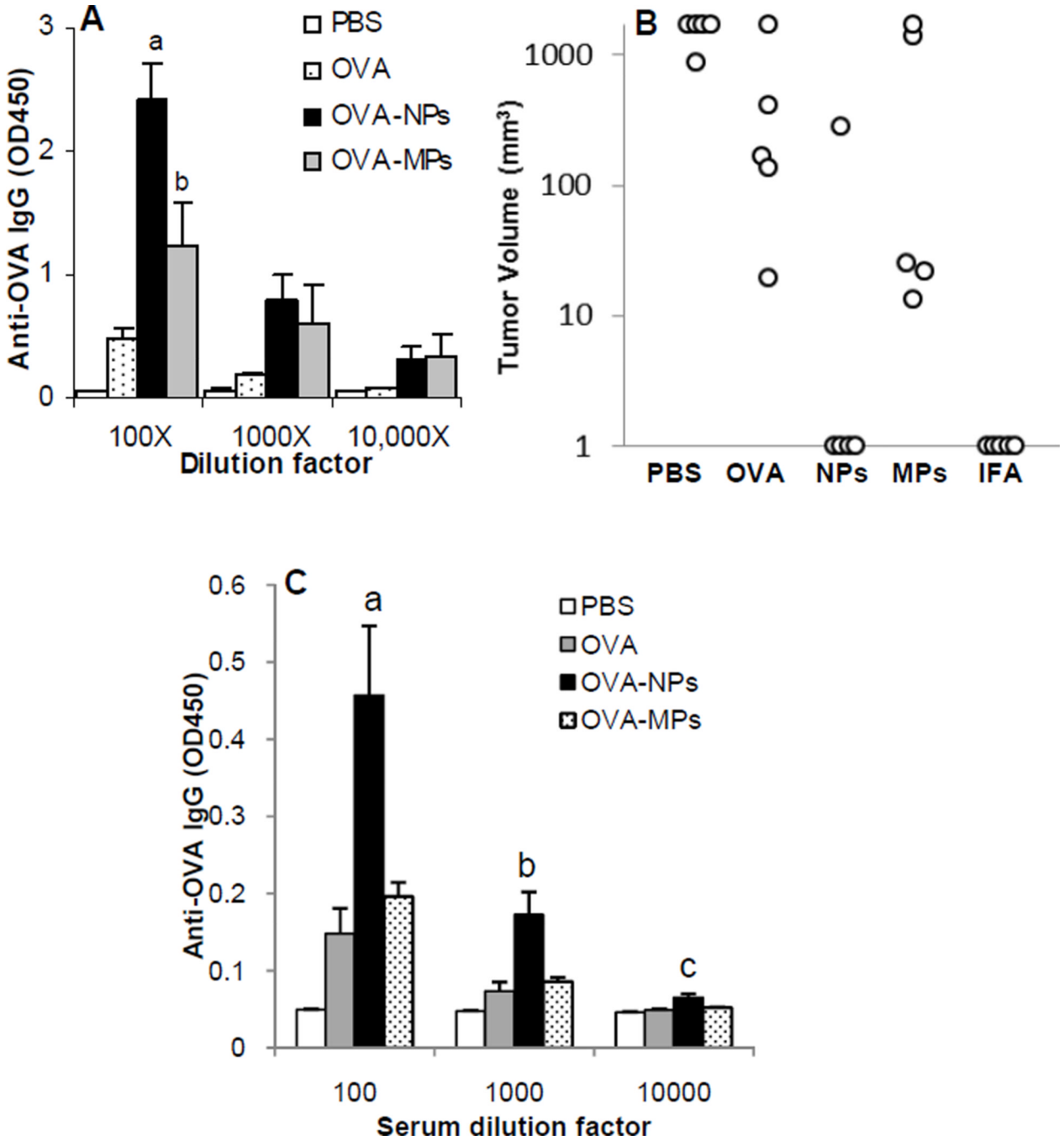

Fig. 3. OVA-adsorbed aluminum hydroxide nanoparticles induced a stronger OVA-specific antibody response and more effectively protected the growth of OVA-expressing tumor cells than OVA-adsorbed aluminum hydroxide microparticles

(A). Serum total IgG response. Mice (n = 5) were dosed with OVA-NPs or OVA-MPs at an OVA to particle ratio of 1:2 (w/w) on days 0, 7 and 14. Total anti-OVA IgG level in serum samples was measured on day 27 ($^{a}p < 0.001$, OVA vs. OVA-NPs; $^{b}p = 0.02$, OVA-NPs vs. OVA-MPs; also, OVA vs. OVA-NPs, p = 0.005 at 1000-fold dilution, p = 0.05 at 10,000-fold dilution).

(B). The volumes of B16-OVA tumors in mice immunized with OVA-NPs or OVA-MPs. Tumor volumes shown are 31 days after tumor cell implantation. B16-OVA tumor cells

were s.c. implanted into mice (n = 5) 10 days after the third immunization. OVA adjuvanted with IFA (OVA/IFA) was a positive control. (Notes: A volume of 1 mm^3 is assigned to mice that do not have tumors because the Y-axis in this figure is in log scale).
(C). Serum total anti-OVA IgG responses. Mice (n = 5) were dosed with OVA-NPs or OVA-MPs at an OVA to particle ratio of 1:5 (w/w) on days 0, 7 and 14. Anti-OVA IgG level in serum samples was measured on day 24 ($^{a-c}p = 0.02$ at all dilutions, OVA-NPs vs. OVA-MPs).

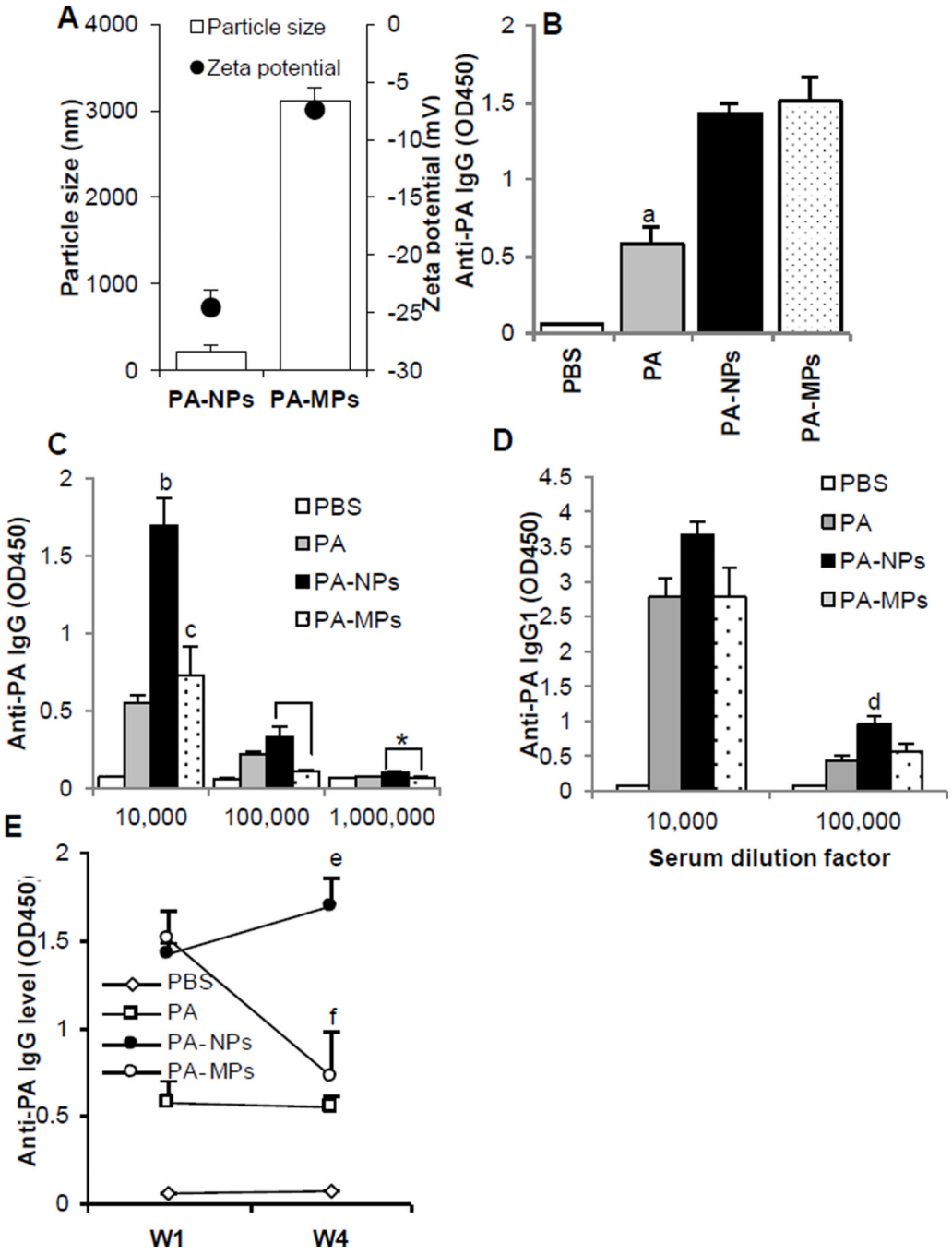

Fig. 4. PA-adsorbed aluminum hydroxide nanoparticles induced a stronger PA-specific antibody response than PA-adsorbed aluminum hydroxide microparticles

(A). Particle sizes (open bar) and zeta potentials (●) of PA-adsorbed aluminum hydroxide nanoparticles (PA-NPs) and PA-adsorbed aluminum hydroxide microparticles (PA-MPs). **(B–D)**. Anti-PA antibody responses. Mice (n = 5) were dosed with PA-adsorbed aluminum hydroxide nanoparticles (PA-NPs) or microparticles (PA-MPs), or PA alone on days 0 and 14 (PA dose, 4 μg per mouse per injection). Anti-PA IgG and IgG1 levels were measured one week (**B**) and four weeks after the second immunization (**C–D**). Data shown in B are anti-PA IgG level in serum samples that were diluted 10,000-fold ($^{a}p = 0.0002$, PA vs. PA-NPs; $p = 0.001$, PA vs. PA-MPs). In C at 10,000-fold dilution, $^{b}p = 0.0002$, PA vs. PA-

NPs; $^{c}p = 0.002$, PA-NPs vs. PA-MPs. * $p = 0.007$, PA-NPs vs. PA-MPs at 100,000-fold dilution; and $p = 0.0002$, PA-NPs vs. PA-MPs at 1,000,000-fold dilution. In D at 100,000 dilution, $^{d}p < 0.05$, PA-NPs vs. PA-MPs.

(E). A comparison of the anti-PA IgG levels in mice one week (W1) and four weeks (W4) after the last immunization (serum samples were diluted 10,000-fold). Data shown are mean ± S.E. (n = 5). $^{e,f}p < 0.05$, week 1 vs. week 4 for both PA-NPs and PA-MPs.

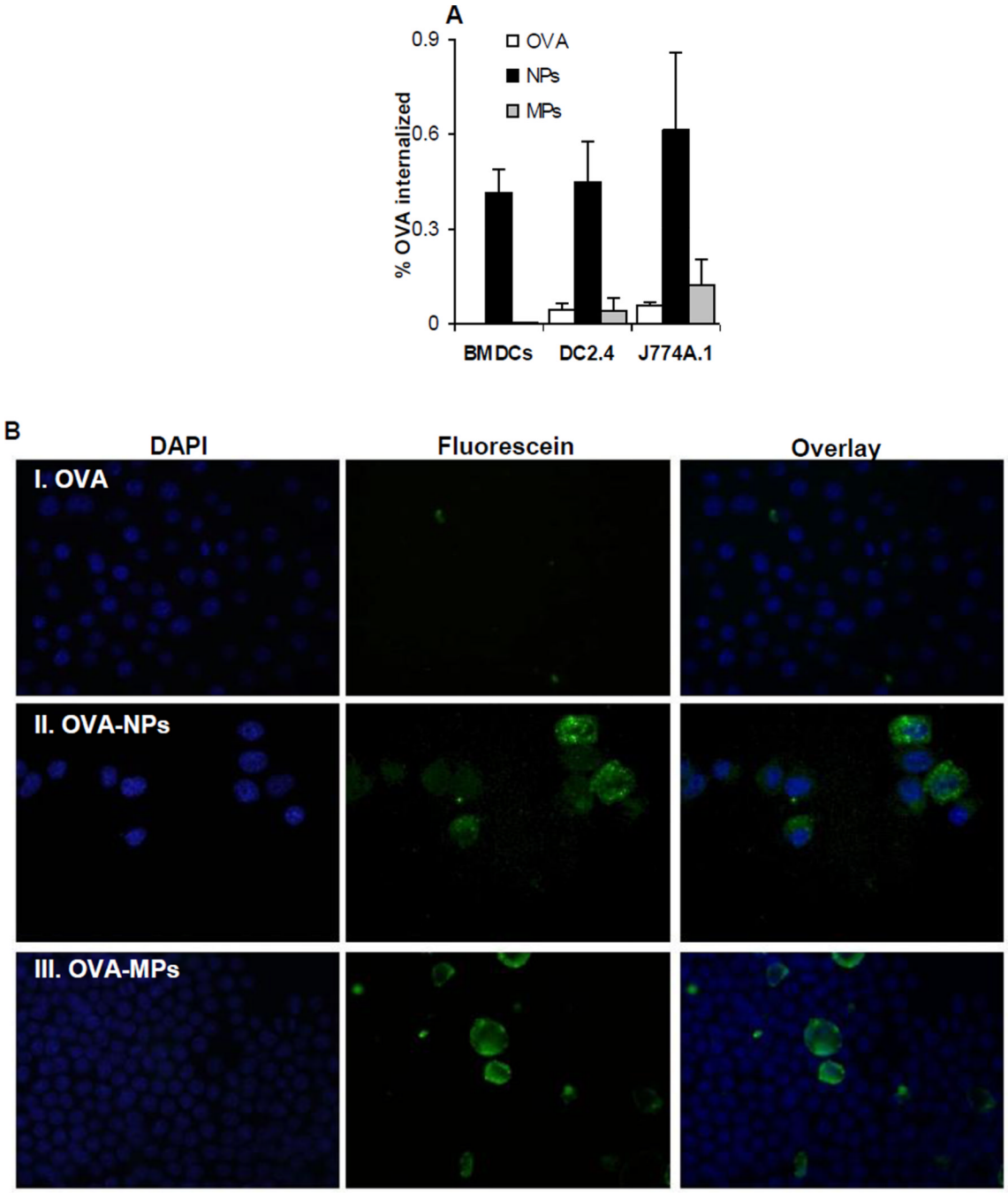

Fig. 5. The uptake of OVA-adsorbed aluminum hydroxide nanoparticles and microparticles

(A) The uptake of OVA-NPs and OVA-MPs by BMDCs, DC2.4, and J774A.1 cells in culture. Aluminum hydroxide nanoparticles or microparticles adsorbed with FITC-labeled OVA were incubated with BMDCs, DC2.4 cells or J774A.1 cells for 3–6 h at 37°C with 5% of CO_2 or at 4°C, and the % of FITC-labeled OVA that was internalized was determined (*$p < 0.05$, OVA-NPs vs. OVA-MPs in all three cells). Data shown are mean ± S.D. ($n = 6$). **(B)**. Representative fluorescence microscopic pictures of DC2.4 cells after incubation with aluminum hydroxide nanoparticles or microparticles pre-adsorbed with FITC-labeled OVA.

(I). FITC-labeled OVA alone; (II). OVA-NPs; (III). OVA-MPs. Cell nuclei were stained with DAPI (blue).

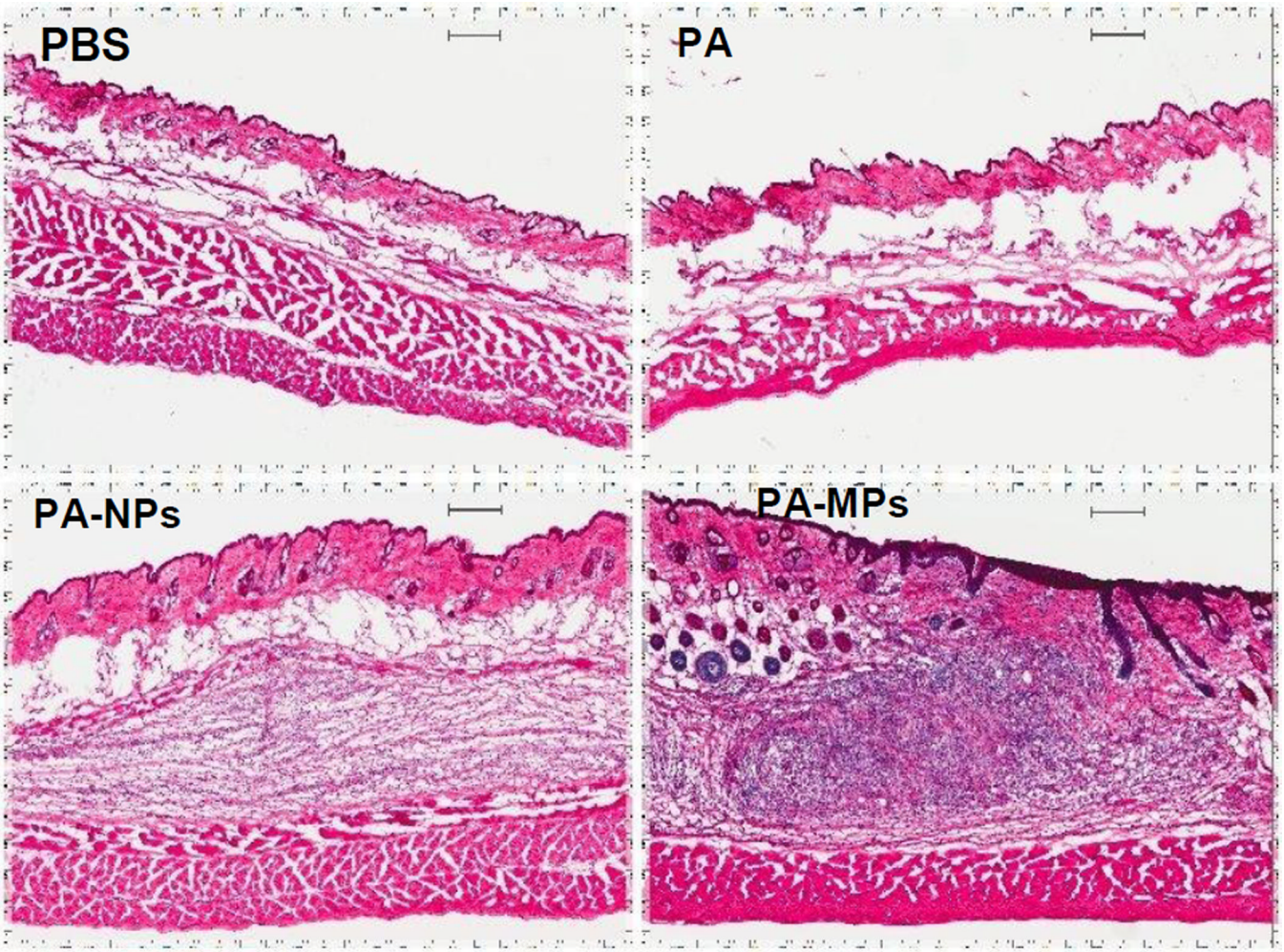

Fig. 6. Representative H&E histograms of the skin in the injection sites

BALB/c mice were s.c. injected with PA-adsorbed aluminum hydroxide particles on days 0 and 19. As negative controls, mice were injected with sterile PBS or PA alone. On day 40, mice were euthanized and the skin samples in the injection sites were collected for cryostat sectioning followed by H&E staining (scale bar, 200 μm).